npj | climate and atmospheric science

www.nature.com/npjclimatsci

ARTICLE OPEN

Check for updates

El Niño and La Niña asymmetry in short-term predictability on springtime initial condition

Hui Chen[1], Yishuai Jin[1,2]✉, Xingchen Shen[3], Xiaopei Lin[1] and Ruikun Hu[4]

El Niño-Southern Oscillation (ENSO) asymmetry in predictability on springtime initial condition remains unclear. From the perspective of the spring predictability barrier (SPB), this paper investigates the ENSO asymmetry in SPB and explores the potential factors that may lead to this asymmetry. Both the observation and 29 Coupled Model Intercomparison Project Phase 6 (CMIP6) models show that the spring sea surface temperature (SST) persistence is significantly higher in El Niño years than that in La Niña years, and the SPB intensity is stronger in La Niña years than that in El Niño years. Through the recharge oscillator model, observation and CMIP6 models, we demonstrate that the nonlinear wind stress response to SST anomalies in spring is the main cause of the asymmetric SPB intensity. By the mixed-layer heat budget of the tropical Pacific in the spring, we further identify that a stronger response of zonal wind stress in El Niño events can cause a stronger zonal advection feedback, which finally leads to a weaker SPB and enhances the predictability of El Niño. In contrast, the cooling SST in the spring only leads to weak easterly anomalies, the zonal advection feedback is relatively weaker, thus SPB is stronger and the predictability of La Niña is lower. From the perspective of SPB, we suggest that El Niño is more predictable than La Niña.

npj Climate and Atmospheric Science (2023)6:121 ; https://doi.org/10.1038/s41612-023-00446-8

INTRODUCTION

El Niño-Southern Oscillation (ENSO) is the dominant mode of interannual climate variability in the tropical Pacific. Its influence has been identified to be worldwide[1,2]. Therefore, it is pivotal to accurately predict ENSO as early as possible due to its tremendous global impact. One major problem in ENSO predictability and prediction is the well-known spring predictability barrier (SPB), which is characterized by a band of maximum decline of monthly predictability (e.g., indicated by autocorrelation) of sea surface temperature (SST; e.g., Niño3.4) anomalies in the boreal spring[3–5]. This maximum decline of ENSO predictability occurs in spring, regardless of different initial months[5,6]. Since then, researchers have begun to more focus on understanding the ENSO SPB[7,8]. Including upper ocean temperatures in the initial conditions can provide an additional skill to cross the boreal spring[7]. Other aspects like westerly wind bursts in the prediction system also significantly increase ENSO prediction skill and weaken the so-called spring prediction barrier[8]. Nevertheless, the SPB is still an obstacle for dynamical and statistical forecasting models even with additional signals from the subsurface temperature in the tropical Pacific[9,10].

The asymmetric characteristic in ENSO predictability remains unclear[11]. Based on observational ENSO precursors, some studies suggested that El Niño is more predictable than La Niña[2]. The similar conclusion through the ensemble forecast experiments can be found in a perfect model framework[12]. Alternatively, some studies demonstrated that strong La Niña events are more predictable because they are mostly driven by the thermocline feedback, while strong El Niño almost are driven by stochastic wind forcing[11,13]. The western Pacific oceanic heat content is a better predictor for La Niña than El Niño[14]. Recently, some studies suggested that El Niño and La Niña events are equally predictable through real-time seasonal ENSO forecasts initialized by oceanic observations[15]. In addition, using Community Earth System Model in a perfect model scenario, researchers demonstrated that additional observations in the equatorial regions may greatly improve El Niño predictions while the observations in the off-equatorial regions around 10°N in the central Pacific may be necessary to improve La Niña predictions[16]. Although much efforts have been made to investigate the predictability of El Niño and La Niña, the asymmetry of ENSO predictability has not been explored from the perspective of SPB. Particularly, we focus on the ENSO asymmetry in short-term predictability on springtime initial condition.

Given that the nonlinear terms have been identified to play a role in ENSO asymmetry[13], these nonlinear terms may also be a reason for ENSO asymmetry in SPB. ENSO nonlinear characteristic of the amplitude, spatial pattern and time evolution are both related to the nonlinear response of the zonal winds to SST anomalies[13,17]. In addition, the nonlinear wind response to SST plays a leading role in the genesis of ENSO asymmetry[18]. However, the role of these terms is yet to be studied in the ENSO asymmetry of predictability.

In this study, we aim to find the ENSO asymmetry of predictability from the view of SPB and demonstrate the possible mechanism to cause this asymmetry. We analyze the SPB intensity of El Niño and La Niña years both in observation and 29 Coupled Model Intercomparison Project Phase 6 models (CMIP6). We then identify the key factors leading to SPB asymmetry in the recharge oscillator model (ROM), observations and CMIP6. A further analysis of the heat budget of the mix layer in the tropical Pacific indicates the specific physical mechanism to induce this asymmetry.

[1]Frontier Science Center for Deep Ocean Multispheres and Earth System (FDOMES) and Physical Oceanography Laboratory, Ocean University of China, Qingdao, China. [2]Open studio for Ocean-Climate-Isotope Modeling, Pilot National Laboratory for Marine Science and Technology (Qingdao), Qingdao 266100, China. [3]Science & Technology on Integrated Information System Laboratory, Institute of Software, Chinese Academy of Sciences, Beijing 100190, China. [4]State Key Laboratory of Satellite Ocean Environment Dynamics, Second Institute of Oceanography, Ministry of Natural Resources, Hangzhou, China. ✉email: jinyishuai@126.com

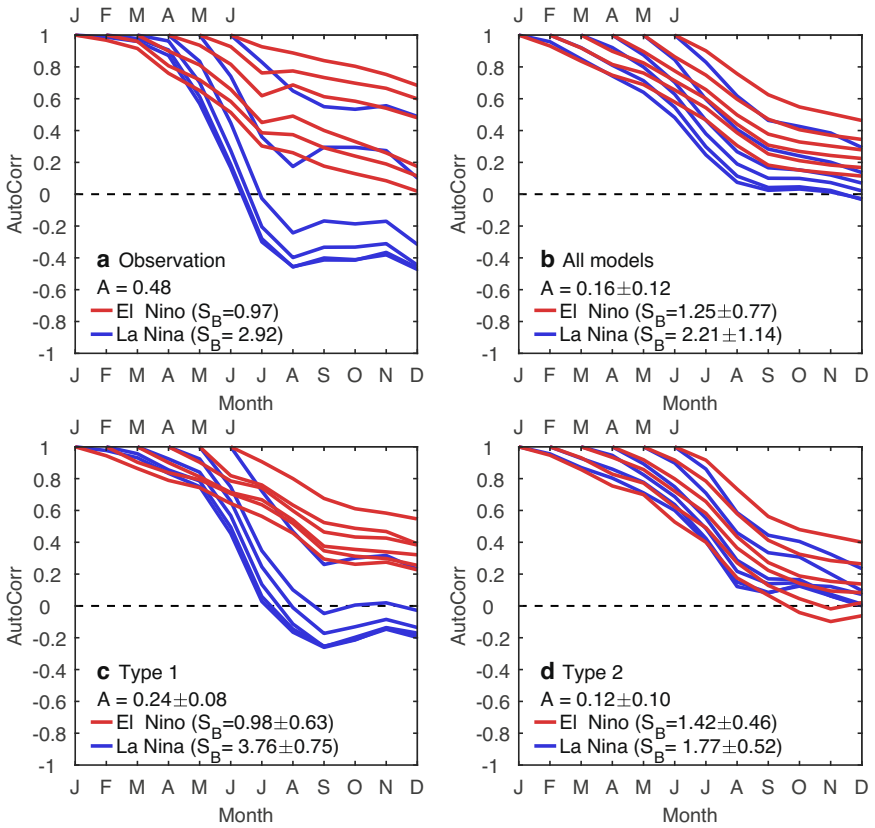

Fig. 1 The SPB in the observation and CMIP6 models. a Autocorrelation calculated by Niño3.4 SST anomalies using observations from 1958 to 2021. Red and blue lines denote El Niño and La Niña years, respectively. The top x axis denotes the initial month and corresponding lag month is marked on the lower axis. **b** Same as **a**, expect for multi-model mean of CMIP6. **c**, **d** Same as **b**, except for type 1 and type 2, respectively. The range of A, SPB for El Niño and La Niña events is the one standard deviation of these models.

RESULTS

ENSO asymmetry of SPB in the observation and CMIP6

A stronger SPB in La Niña years than that in El Niño years can be found in the observation (Fig. 1a). In general, the autocorrelation decreases dramatically from March (especially from April) to June (Supplementary Fig. 1a) for different initial months, indicating that SPB is a distinct feature, regardless of the different ENSO states. Here we mainly focus on the persistence change in April (0) to June (0). To investigate the SPB under different ENSO states, we choose El Niño and La Niña years from 1958 to 2021 and obtain the autocorrelation function, respectively. In El Niño years, regardless of the initial months, the persistence drops relatively slowly before March (0) and exhibits relatively sharp drop-offs after March (0) (Fig. 1a; Red lines). Its SPB intensity is 0.97 (i.e., $S_B = 0.97$; the definition of SPB intensity is shown in the Methods). Compared with El Niño years, the persistence declines more slowly before April (0) but drops more sharply after April (0) in La Niña years (Fig. 1a; Blue lines). As such, the SPB intensity in La Niña years is significantly stronger ($S_B = 2.92$; the way of significant test by Monte Carlo can be checked in the Methods). Different definitions of ENSO years do not change the results. Moreover, the asymmetry of SPB also exists when we only use the first year of multi-year ENSO events (see also Supplementary Fig. 2). In summary, ENSO events exist an asymmetric characteristic in SPB intensity, i.e., the barrier is stronger in La Niña years than that in El Niño years.

The CMIP6 datasets also identify that the SPB in El Niño years is much weaker than La Niña years (Fig. 1b). From the multimodel mean of the 29 CMIP6 models, in El Niño years, regardless of the initial months, the persistence drops relatively slowly before May (0) and exhibits relatively sharp drop-offs after May (0) (Fig. 1b; Red lines). Its SPB intensity is 1.26 (i.e., $S_B = 1.25$). Compared to El Niño years, the persistence drops relatively slowly before May (0) and exhibits sharper drop-offs after May (0) (Fig. 1b; Blue lines) in La Niña years ($S_B = 2.21$). 29 CMIP6 models also identify a stronger SPB for La Niña than that for El Niño, which is consistent with observations (Fig. 1a vs. Figure 1b). Only 6 models (21%) indicate a weaker SPB of La Niña (Supplementary Fig. 3a). Note here the asymmetry of SPB is also strong when we only use the first of ENSO years in CMIP6 models (Supplementary Fig. 3b). In the rest of 23 models, some models (e.g., CNRM-ESM2-1) show a stronger asymmetry of SPB. The difference of the SPB index is larger than 2. Meanwhile, some models (e.g., CESM2-WACCM) exhibits a weaker asymmetry and the difference is smaller than 0.5. As such, we choose two types of models in these models according to the asymmetry of SPB: type 1 is the models that shows a significantly stronger SPB of La Niña than El Niño (Fig. 1c; i.e., top-five SPB difference models among 23 climate models; Table 1) while type 2 is the situation when the difference of SPB between El Niño and La Niña is modest (Fig. 1d; i.e., bottom-five SPB difference models among 23 climate models; Table 1). The difference of type 1 and type 2 can be used to identify the possible physical mechanism indicated by the observation. A point to be returned later.

Asymmetric ENSO SPB in the ROM

To identify the key factor leading to SPB asymmetry, we use a simple ROM (the ROM can be found in the Methods)[18–20]. We first add the seasonal cycle of growth rate ($R_0 \neq 0$) to exhibit the ENSO SPB feature, which is consistent with previous studies[4,6,21]. The persistence drops dramatically from March to June. However, the SPB intensity is almost equal for El Niño ($S_B = 1.61$) and La Niña ($S_B = 1.60$), which indicates that the ENSO asymmetry of SPB does

not exist (Fig. 2a). This is because the asymmetric feature is not introduced in the model. In this case, El Niño and La Niña are symmetrical.

To further demonstrate the asymmetrical feature of ENSO in ROM, we add the nonlinear terms in the model. Previous studies suggested that the nonlinear wind stress response to SST anomalies (atmospheric nonlinear feedback) can induce oceanic nonlinear feedbacks and dominates the genesis of ENSO asymmetry[18]. Therefore, we introduce the term of nonlinear wind stress response to SST into ROM and explore the role of this term on SPB asymmetry. To incorporate the nonlinear atmospheric feedback (β_1) into the model, we adopt a simple piecewise form of τ to T[18],

$$\tau = a_3(T + \beta_1|T|) + \xi \quad (1)$$

We then set $\beta_1 > 0$ (a stronger wind stress response of warm SST anomalies than that of cold SST anomalies), which represents the presence of nonlinear wind stress response to SST anomalies in the tropical Pacific. It turns out that when $\beta_1 > 0$ (the nonlinear wind stress response to SST exists), the SPB intensity of La Niña ($S_B = 1.82$) is obviously stronger than that of El Niño ($S_B = 1.45$; Fig. 2b). Note here although the nonlinearity of wind stress response (i.e., Eq. (1)) does not vary seasonally, its effect has the seasonality due to the seasonal cycle of growth rate (Supplementary Fig. 4). Moreover, the seasonality of β_1 does not dramatically change the asymmetry of SPB (Supplementary Fig. 5). The role of nonlinear wind stress response of SST in SPB asymmetry can be further identified in Fig. 2c. When β_1 increase from 0 to 0.6, the strength of SPB gets larger for La Niña events but becomes weaker for El Niño events (Blue vs. Red line in Fig. 2c). Specifically, the difference of SPB intensity between El Niño and La Niña increases when β_1 gets larger. According to Eq. (1), when β_1 get larger, for $T > 0$, it means that a stronger westerly anomalies response ($T > 0$ and $\beta_1|T| > 0$ in Eq. (1)). This may induce the El Niño events afterwards and the SPB strength is weaker. On the other hand, for $T < 0$, it indicates that a weaker easterly anomalies response ($T < 0$ but $\beta_1|T| > 0$ in Eq. (1)), indicating a stronger SPB strength for La Niña events. Many other factors may also lead to ENSO asymmetry of SPB[6,18,22,23], including the initial conditions (Supplementary Fig. 6). By using the various kinds of recharge oscillator models, we find that the asymmetrical response of wind stress is an essential factor for ENSO asymmetry of SPB (See Supplementary Figs. 7 and 8).

By preforming the forecast in the ROM (more details for the prediction can be checked in the Methods), we further identify the asymmetrical predictability of ENSO both in the perfect model and real-world frameworks. In the perfect model framework, when $\beta_1 = 0$ (Fig. 2d), both the El Niño and La Niña events exhibit similar drop of prediction skill in anomaly correlation coefficient (ACC) during the spring, indicating that there is no asymmetry of predictability. When $\beta_1 = 0.6$ (Fig. 2e), the ACC of El Niño drops more slowly during the spring compared with La Niña. For the

Table 1. The CMIP6 models of Type1 and Type2.

Type1	Type2
CNRM-ESM2-1	CAS-ESM2-0
EC-Earth3-CC	CESM2-WACCM
EC-Earth3-Veg-LR	GFDL-ESM4
FGOALS-g3	MPI-ESM1-2-HR
INM-CM5-0	UKESM1-0-LL

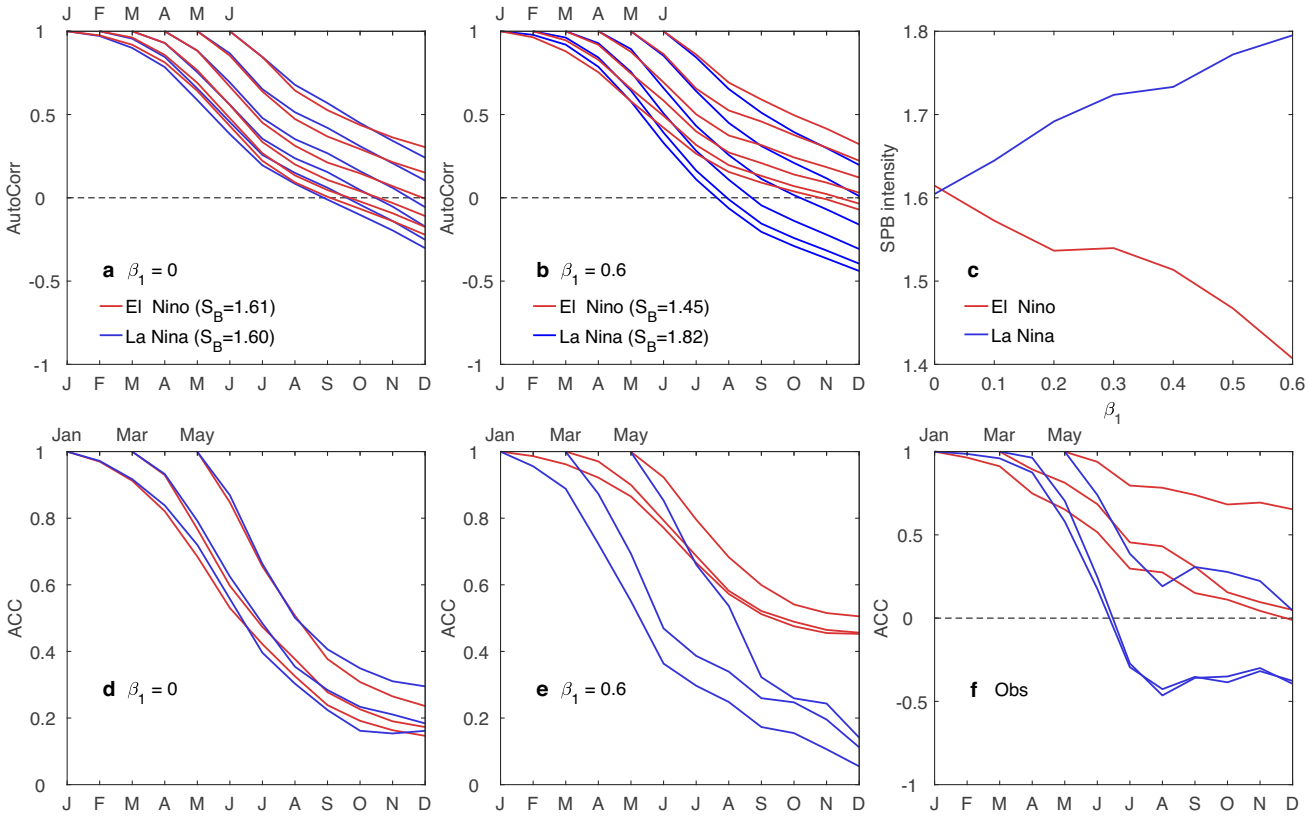

Fig. 2 The SPB in the ROM. a Same as Fig. 1a, expect for the results from ROM where $\beta_1 = 0$. **b** Same as **a** except for $\beta_1 = 0.6$. **c** The modulation of SPBs under different β_1 in ROM. **d** In the perfect model framework, the anomaly correlation coefficient (ACC) of the forecasts starting from different initial months when $\beta_1 = 0$ in the ROM. The red and blue lines represent the El Niño and La Niña years, respectively. **e** Same as **d**, except for $\beta_1 = 0.6$. **f** Same as **e**, expect we use ROM to forecast the observation. using observation as "truth", respectively.

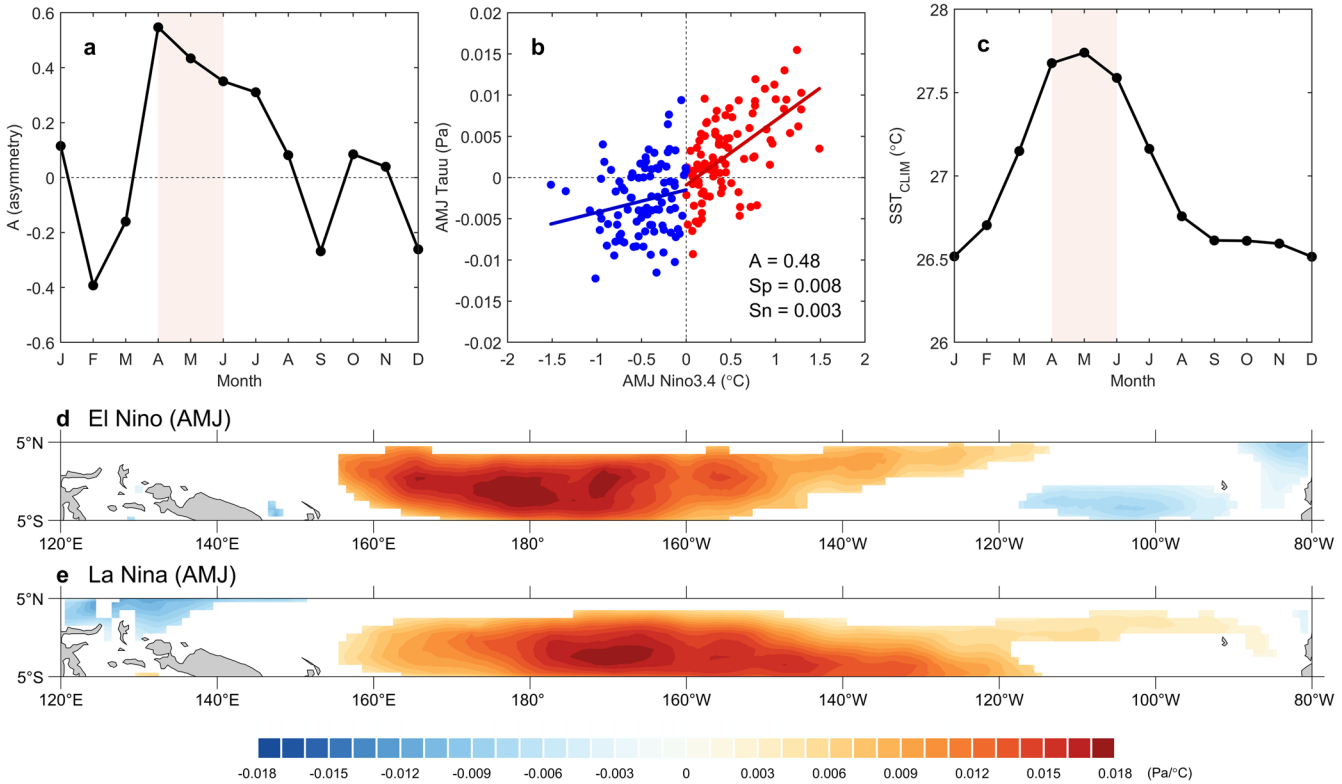

Fig. 3 The nonlinear wind stress response of SST in the observation. a The seasonality of A. **b** Scatter diagram of Niño 3.4 index and zonal wind stress (Tauu; averaged from 120°E-80°W, 5°S-5°N) from April to June. Red dots represent the response of zonal wind stress to warm SST anomalies. Blue dots are same as red dots, expect for the response on cold SST anomalies. The red line and blue lines are the regression line for this relationship with S_p is the regression coefficient for red dots and S_n for blue dots, respectively. **c** The background of the SST in the Niño 3.4 region for different calendar months. **d** Regressions of spring (AMJ) tropical Pacific zonal wind stress anomaly of El Niño years onto corresponding Niño3.4 index. Only the regression coefficient exceeding 95% confidence level is shown in the figure. **e** Same as **d**, except for the La Niña years.

real-world framework, the way we perform forecasts is the same as what we do in the perfect model framework, expect that we use observation as the "truth". The ACC of El Niño also drops more slowly during the spring compared with La Niña in Fig. 2f. Note here the asymmetry of SPB also exists when $\beta_1 = 0$ for the real-world forecasts, which indicates the importance of the initial conditions (Supplementary Fig. 6). As such, the weaker SPB of El Niño than La Niña also indicates a higher predictability of El Niño than La Niña when the initial month is in the spring. Usually, El Niño starts earlier than La Niña and its SPB is supposed to be low.

A possible mechanism to explain the ENSO asymmetry in SPB both in the observation and CMIP6

The nonlinear response of zonal wind stress on SST anomalies can also be found in the observations, especially in the spring. This asymmetric response of zonal wind stress on SST anomalies (i.e., *A*) is more evident in April to June than in other months (Fig. 3a; see Methods for calculation). Particularly, in AMJ, warm SST anomalies generate stronger anomalous westerlies (with a slope as 0.008 Pa $°C^{-1}$; i.e., $S_p = 0.008$; Fig. 3b) while cold SST anomalies generate weaker easterlies anomalies (with a slope as 0.003 Pa $°C^{-1}$; i.e., $S_n = 0.003$). This asymmetry, which is indicated by *A*, is 0.48. These different responses of the wind stress may be caused by the background of the SST in the tropical Pacific (Fig. 3c). During the spring (AMJ), the averaged SST are larger than other months. This warmer SST is easier to induce stronger zonal wind stress anomalies[24]. Note here that the nonlinear wind response affects the asymmetry of the ENSO growth rate in spring, thus contributing to SPB asymmetry.

This point can be identified by regressing zonal wind stress anomalies onto the Niño3.4 index for El Niño and La Niña years, respectively (Fig. 3d, e). It is found that the response of spring zonal wind stress anomaly on SST anomalies in El Niño years (Fig. 3d) is stronger than that in La Niña years (Fig. 3e), especially in the western and central tropical Pacific. This area has been shown to be important for air-sea coupling and ENSO events[25]. Hence, a stronger response of wind stress during the spring El Niño years leads to a weaker SPB and a higher predictability of El Niño. We will further show in the next section that the zonal current response is stronger when the zonal wind stress anomaly is positive and thus the zonal advective feedback is essential for the asymmetry of SPB.

A further analysis of the CIMP6 models also identify the relationship between the nonlinear wind stress responses and SPB. Note here both the ENSO events SPB and overall SPB (Fig. 1b and Supplementary Fig. 1b) in the CMIP6 are more prominent from May to July, which lags the observation for one month. It may be caused by the failure of the simulation of CMIP6 for the climatology (e.g., the cold bias in the eastern Pacific for CMIP6)[26]. Hence, we identify the nonlinear response of wind stress from May to July in CMIP6 to explain the relationship between the nonlinear response and SPB. First, the overall CMIP6 models underestimate the asymmetry of the wind stress response (i.e., $A = 0.16$, which is smaller than the observation, i.e., $A = 0.48$). By dividing CMIP6 models into two types (Fig. 1c, d), we find that the asymmetric wind stress response of type 1 ($A = 0.24$), which is significantly stronger SPB for La Niña years than El Niño years, is larger than that of type 2 ($A = 0.12$). To further identify the role of the asymmetrical wind stress response, the relationship between the

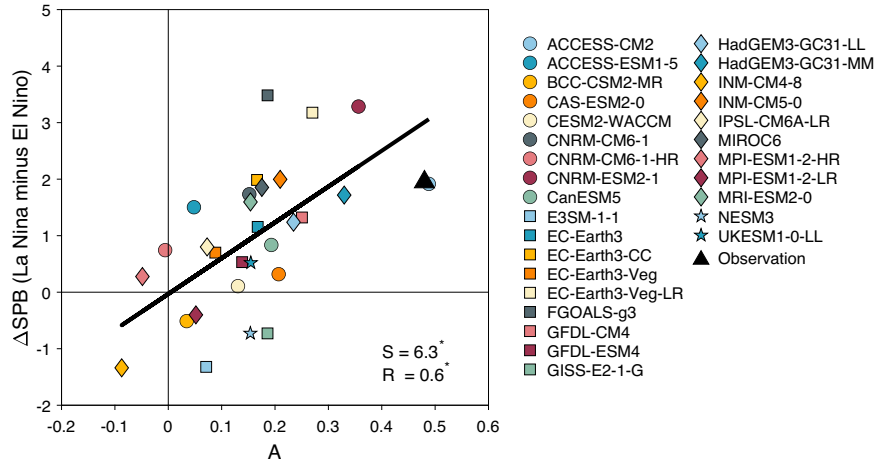

Fig. 4 Intermodel relationship between MJJ nonlinear wind stress response and the SPB difference between La Niña and El Niño (ΔSPB). The black line is the regression line, with the regression coefficient $S = 6.3$. The correlation coefficient $R = 0.6$. The '*' denotes that the correlation coefficient and the slope exceed 95% confidence level.

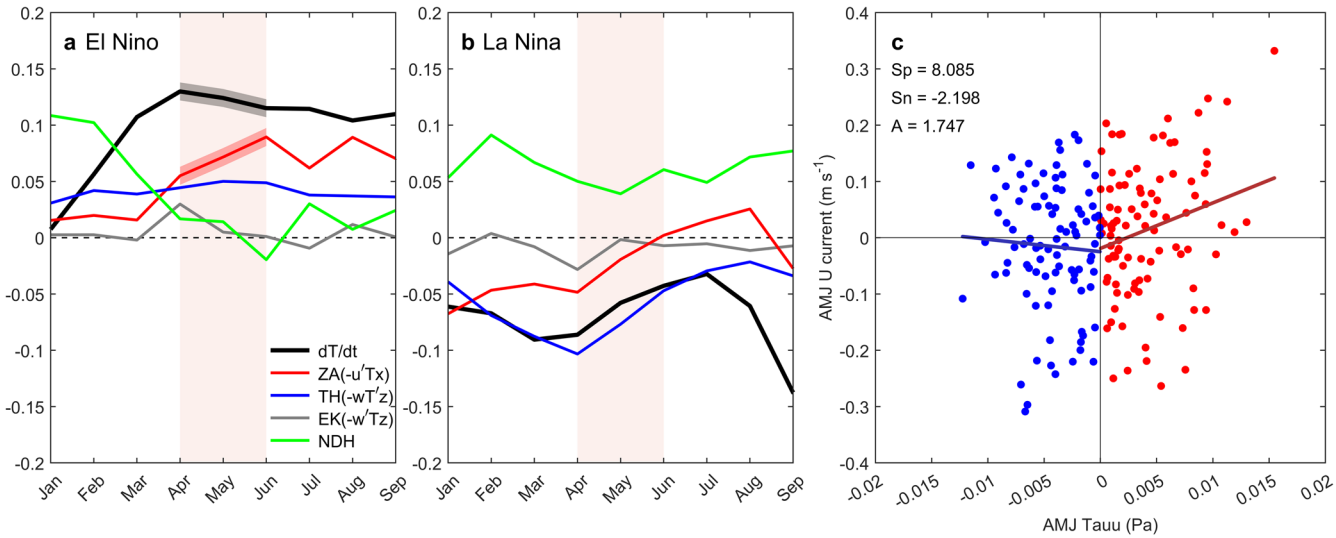

Fig. 5 The mixed-layer temperature tendency terms. a Composites of each term in the SST equation for the El Niño years. Black line indicates SST tendency. Red, blue, gray and green lines indicate ZA, TH, EK feedback and nonlinear dynamic heating. **b** Same as **a**, except for the La Niña years. **c** Same as Fig. 3b, expect for the scatter diagram of equatorial mean (120°E-80°W, 5°S-5°N) zonal wind stress and zonal current. The black and red shading in **a** indicate the difference of dT/dt and ZA feedback ($-u'\frac{\partial \overline{T}}{\partial x}$) term in spring (AMJ) between the El Niño and La Niña is statistically significant at more than 95% confidence level (using bootstrap test; see method).

A index and the asymmetry of SPB is suggested using 29 CMIP6 models. It is shown that the *A* index is significantly related to the asymmetry of SPB. When *A* is larger, the asymmetry of SPB is also stronger (Fig. 4). As such, a larger asymmetrical SPB is caused by a stronger nonlinear response of wind stress to SST anomalies in the tropical Pacific.

The specific feedback causes the SPB asymmetry

To examine the specific feedback contributes to SPB asymmetry as the wind stress anomalies can lead to three different positive feedbacks, a budget analysis of the mixed layer temperature is performed (see Methods). We mainly focus on the terms of zonal advection feedback (ZA; $-u'\frac{\partial \overline{T}}{\partial x}$), thermocline feedback (TH; $-\overline{w}\frac{\partial T'}{\partial z}$), Ekman feedback (EK; $-w'\frac{\partial \overline{T}}{\partial z}$) which closely related to zonal wind stress and the terms of nonlinear dynamic heating (NDH; $-u'\frac{\partial T'}{\partial x}-v'\frac{\partial T'}{\partial y}-w'\frac{\partial T'}{\partial z}$), which plays a role on ENSO asymmetry. Other terms are relatively small (Supplementary Fig. 9).

The asymmetry of ZA is essential for the development speed of El Niño and La Niña years and the asymmetry of SPB (Fig. 5). During April to June, the warming tendency of the Niño3.4 SST for El Niño years (Fig. 5a; Black line) is significantly stronger than that for La Niña years (Fig. 5b; Black line; Bootstrap test, see method), indicating that the development of El Niño is faster than La Niña and thus a weaker SPB for El Niño. Meanwhile, ZA feedback, indicated by the anomalous current and climatological SST zonal gradient, significantly contributes to the SST warming tendency in AMJ for El Niño years (red line in Fig. 5a). Compared to El Niño years, this term is relatively small in AMJ for La Niña years (red line in Fig. 5b). As such, the asymmetry of ZA leads to the different development speeds of ENSO years. In AMJ, the TH feedback, which suggests the anomalous temperature advected by the climatological upwelling, show no significant difference in El Niño and La Niña years. We also use another definition of TH and find the asymmetry of TH term is also small during the spring[27,28]. Hence, the nonlinear wind stress response in the tropical Pacific,

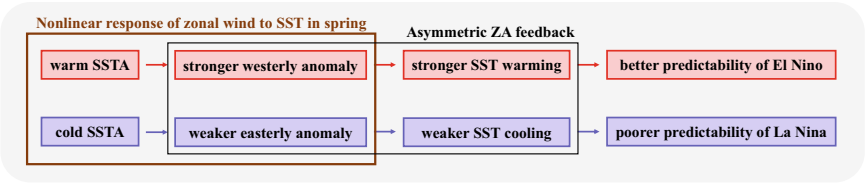

Fig. 6 Schematic mechanism of SPB asymmetry. The anomalous SST warming will cause strong westerly anomalies, strong zonal current anomalies and further strengthen the initial SST warming. As such, a larger El Niño growth rate will lead to a stronger ZA positive feedback, a weaker SPB and higher El Niño predictability. Nevertheless, the easterly anomalies caused by SST cooling are relatively weaker compared to westerly anomalies, so does the ZA feedback and La Niña growth rate. Hence, it leads to a stronger SPB and lower predictability of La Niña.

leads to a stronger ZA feedback for El Niño than that for La Niña years during the boreal spring to the early summer, finally causes the asymmetry of SPB. Note here the NDH term also shows a positive tendency in El Niño and La Niña years, indicating that this term always plays a warming role on SST anomalies. The role of NDH in the asymmetry of SPB needs a further study.

We further show that why ZA instead of TH is essential for the asymmetry of SPB. The air-sea coupling strength contains two aspects. One is the sensitivity of the wind stress to SST anomaly, the other one is the sensitivity of the oceanic response to wind stress. We find that the sensitivity of thermocline response in the tropical Pacific are similar for the positive and negative wind stress ($A = 0.057$; Supplementary Fig. 10). However, the zonal current response is asymmetrical ($A = 1.747$). Particularly, when the zonal wind stress is positive during the spring, the zonal current response is significantly stronger than the cases when the zonal wind stress is negative (Fig. 5c). Thus, the zonal advective feedback is asymmetrical and leads to asymmetry of ENSO SPB.

The role of this nonlinear response can be indicated schematically in Fig. 6. The anomalous SST warming will cause strong westerly anomalies, strong zonal current anomalies and further strengthen the initial SST warming. As such, a larger El Niño growth rate will lead to a stronger ZA positive feedback, a weaker SPB and higher El Niño predictability. Nevertheless, the easterly anomalies caused by SST cooling are relatively weaker compared to westerly anomalies[18], so does the ZA feedback and La Niña growth rate. Hence, it leads to a stronger SPB and lower predictability of La Niña.

DISCUSSION

In this paper, we explore the ENSO asymmetry in SPB and propose a mechanism to explain this asymmetry. Observed ENSO events exhibit an asymmetric characteristic in SPB intensity. In particular, the SPB in El Niño events is weaker than that in La Niña events. This can also be identified using CMIP6 datasets. The ROM is then used to investigate the ENSO asymmetry of SPB intensity. Nonlinear term β_1, which is related to nonlinear wind stress response to SST, is the main cause of asymmetric ENSO predictability. Moreover, the SPB asymmetry becomes greater with the increase of β_1. The nonlinear response of zonal wind stress on SST anomalies may affect the asymmetry of the ENSO growth rate in spring and contribute to SPB asymmetry, which is identified both in the observation and CMIP6. The stronger westerly anomalies caused by anomalous SST warming further strengthen the initial SST warming through ZA feedback. This will cause a larger ENSO growth rate, a weaker SPB and enhance the predictability of El Niño. On the contrary, the easterly anomalies caused by SST cooling and the oceanic zonal current response to wind stress anomalies are relatively weaker. Thus, the initial SST cooling cannot be effectively enhanced due to the weaker ZA feedback. This leads to a smaller ENSO growth rate, a stronger SPB and lower predictability of La Niña events.

In addition to the asymmetry in SPB, the SPB of El Niño diversity may also exist because of the relationship between SST and anomalous wind patterns. Recent studies have shown that the large differences in spatial pattern from event to event for El Niño[29,30]. The different SST patterns are associated with different anomalous wind patterns, which may also lead to the SPB of El Niño diversity. For example, El Niño events with their largest anomalies in the central equatorial Pacific may have weaker wind anomalies confined to the western part of the basin, which may result in less persistence. The El Niño diversity in SPB should be explored in our further study.

North Pacific Meridional mode (NPMM) may also lead to the asymmetry of ENSO SPB. A stronger NPMM may occur during the El Niño years, which may in turn cause a stronger wind anomaly by Wind-Evaporation-SST feedback[31,32] and a weaker SPB. As the NPMM cannot be included in the simple ROM, a further study using fully coupled general circulation model is needed to check the role of NPMM.

We should bear in mind that the asymmetry of ENSO predictability may behave in an opposite way from different perspectives at different lead times. For example, western Pacific oceanic heat content is a better predictor to La Niña than that of El Niño[11,14]. That is, La Niña is more predictable from ocean heat content perspective beyond 1-year lead. Note here we emphasize the role of SPB and thus the initial month is in the boreal spring (i.e., the lead time is shorter than 8 months). Longer predictability of ENSO comes from oceanic heat content while shorter predictability is originated from the SST persistence (Supplementary Fig. 11). How to estimate ENSO predictability from different perspectives at different lead times still needs a thorough study.

METHODS

Observational data and identifying ENSO events

The monthly data (SST, zonal wind stress and depth of 20°C isotherm) from 1958 to 2021 is obtained from the European Centre for Medium-Range Forecasts Ocean Reanalysis System 5 (ORAS5)[33]. To calculate the oceanic mixed-layer heat budget, SODA 2.2.4 (Simple Ocean Data Assimilation, 0.5°lat × 0.5°lon, from 1958 to 2001) ocean data are used[34].

All monthly mean data are used after the climatological seasonal cycle and linear trends being removed. El Niño (La Niña) events are defined as SST anomalies of Niño3.4 (170°W–120°W, 5°N–5°S) in December(0)–January–February(1) exceeding 0.5 (-0.5) °C in observation, 1 (-1) of normalized SST anomalies of Niño3.4 in the CMIP6 or one positive (negative) standard deviation of SST anomalies in ROM (Table 2)[20].

The definition of SPB intensity

In this paper, ENSO SPB strength can be defined as follows. Taking El Niño years as an example. During the El Niño years (0), for a given initial month (t; ranging from January to May in this year (0)) and the target month τ, we calculate the autocorrelation function r(t,τ) using all El Niño events. For every initial month t, we identify

Table 2. ENSO years (Year 0).

El Niño	La Niña
1963 1965 1968 1969 1972 1976 1977 1982 1986 1987 1991 1994 1997 2002 2006 2009 2014 2015 2018	1964 1970 1971 1973 1974 1975 1983 1984 1985 1988 1995 1996 1998 1999 2000 2005 2007 2008 2010 2011 2017

Table 3. ROM parameter and corresponding value.

Parameter	Value
R_a	-0.19 month^{-1}
R_0	-0.25 month^{-1}
a_{12}	0.02 °C m^{-1} month^{-1}
a_{13}	3.38×10^{-12} °C m month kg^{-1}
a_{21}	-1.415 m °C^{-1} month^{-1}
a_3	2.92×10^{10} kg m^{-1} month^{-1} °C^{-1}
ω_a	2π/12 month^{-1}
φ	0.13

$S_{B1}(t)$ as the specific SPB strength which is calculated as:

$$S_{B1}(t) = \begin{cases} r(t, Apr(0)) - r(t, Jun(0)), t < May(0) \\ r(t, May(0)) - r(t, Jun(0)), t = May(0) \end{cases} \quad (2)$$

The total intensity of the SPB is estimated as:

$$S_B = \sum_{t=Jan(0)}^{May(0)} S_{B1}(t) \quad (3)$$

In order to test the significance of the SPB intensity difference between El Niño and La Niña years, the Monte Carlo method is used as follows: We disorder the time series of El Niño and La Niña years in the observations for 10,000 times in random and calculate 10,000 SPB intensities. The 10000 SPB difference between El Niño and La Niña can determine 95% confidence intervals (the difference > |1.55| is significant) for the difference between El Niño and La Niña SPB in observation.

Normalized asymmetricity

In order to quantitatively measure the nonlinearity existent in the air-sea coupled process[35], we define a normalized asymmetricity as:

$$A = \frac{S_p - S_n}{S_p + S_n} \quad (4)$$

where S_p and S_n represent the slopes for the positive and negative cases, respectively.

The Recharge Oscillator Model and predictions

We adopt ROM to further investigate the SPB asymmetry phenomenon in observation[18–20,36].

$$\frac{dT}{dt} = RT + a_{12}h + a_{13}\tau \quad (5)$$

$$\frac{dh}{dt} = a_{21}T \quad (6)$$

$$\tau = a_3 T + \xi \quad (7)$$

$$R = R_a + R_0 \sin(\omega_a t - \varphi) \quad (8)$$

Note here R is seasonally varying as the seasonal cycle of ENSO growth rate is the cause of SPB[21]. The variable T is chosen as representing the Niño3.4 (170°W–120°W, 5°N–5°S) SST anomaly, as it captures both the warm and cold ENSO events in observation. h and τ denote the equatorial averaged thermocline and zonal wind stress anomalies in the Pacific (120°E–80°W, 5°N–5°S), respectively. Note here the wind stress and the damping term of h in Eq. (6) are omitted as these terms are small[37]. All the numerical results presented in this paper are calculated from the last 2000 years of a 2050-year run. The numerical models are solved in a time step of 0.3 days. Model parameters can be estimated from observations using multilinear regression method (Table 3).

We also perform ensemble forecasts in the ROM to compare the prediction skill of different initial month both in the perfect model and real-world frameworks. The parameters in ROM are obtained by the regression through the observations, which are consistent with previous study[13]. For perfect model framework, we use control run as the "truth". We do ensemble forecasts in every month of 2000 years with 12 months forecast length to get sufficient forecast data. For each of the forecast ensemble members (20 members), a small random normal perturbation (zero mean and 0.1 times standard deviation of T) is added to variable T as the initial condition[38]. The real-world framework is the same with perfect model framework, expect that we treat observation from 1958 to 2021 as "truth".

In this study the forecast skill is verified using the ACC. ACC is defined as the temporal correlation coefficient between ensemble mean forecast and the corresponding "truth"[39]:

$$\mathrm{ACC} = \frac{<F_i, O_i>}{\sqrt{<F_i, F_i> * <O_i, O_i>}} \quad (9)$$

where F_i is the ensemble mean forecast anomaly for forecast month or year i, and O_i is the verifying observed anomaly. < > denotes the variance over all the months or years in verifying time series.

The oceanic mixed-layer heat budget

To understand the relative roles of ocean dynamics (i.e., three-dimensional temperature advection) in causing the SPB asymmetry between composite El Niño and La Niña episodes, we analyze the oceanic mixed layer heat budget in Niño3.4 region. The mixed layer temperature anomaly (MLTA) tendency equation may be written as follows[40]:

$$\begin{aligned} \frac{\partial T'}{\partial t} = & -u'\frac{\partial \overline{T}}{\partial x} - \overline{u}\frac{\partial T'}{\partial x} - u'\frac{\partial T'}{\partial x} - v'\frac{\partial \overline{T}}{\partial y} - \overline{v}\frac{\partial T'}{\partial y} \\ & - v'\frac{\partial T'}{\partial y} - w'\frac{\partial \overline{T}}{\partial z} - \overline{w}\frac{\partial T'}{\partial z} - w'\frac{\partial T'}{\partial z} + \mathrm{Re} \end{aligned} \quad (10)$$

where T denotes the mixed layer temperature; u, v, and w represent three-dimensional (3D) ocean currents; $\partial/\partial x$, $\partial/\partial y$, and $\partial/\partial z$ denote the 3D gradient operator; a prime represents the interannual anomaly; a bar represents the climatological mean state; and the first nine terms on the right-hand side of the equation are 3D temperature advection terms[41]. Re denotes the residual term. All the mixed layer terms in the equation above are calculated based on the vertical average within the mixed layer.

CMIP6 models

To complement the insufficient sample of observations in the asymmetry of SPB, we also analyze the monthly data of 29 CMIP6 (Table 4) in historical simulations from 1900 to 2014[42]. All monthly mean data are used after the climatological seasonal cycle and quadratically trends being removed. The SST anomalies of Niño3.4 are normalized.

Table 4. The CMIP6 models.

Model Name	Ensemble member
ACCESS-CM2	r1i1p1f1
ACCESS-ESM1-5	r1i1p1f1
BCC-CSM2-MR	r1i1p1f1
CAS-ESM2-0	r1i1p1f1
CESM2-WACCM	r1i1p1f1
CNRM-CM6-1	r1i1p1f2
CNRM-CM6-1-HR	r1i1p1f2
CNRM-ESM2-1	r1i1p1f2
CanESM5	r1i1p1f1
E3SM-1-1	r1i1p1f1
EC-Earth3	r1i1p1f1
EC-Earth3-CC	r1i1p1f1
EC-Earth3-Veg	r1i1p1f1
EC-Earth3-Veg-LR	r1i1p1f1
FGOALS-g3	r1i1p1f1
GFDL-CM4	r1i1p1f1
GFDL-ESM4	r1i1p1f1
GISS-E2-1-G	r1i1p1f2
HadGEM3-GC31-LL	r1i1p1f3
HadGEM3-GC31-MM	r1i1p1f3
INM-CM4-8	r1i1p1f1
INM-CM5-0	r1i1p1f1
IPSL-CM6A-LR	r1i1p1f1
MIROC6	r1i1p1f1
MPI-ESM1-2-HR	r1i1p1f1
MPI-ESM1-2-LR	r1i1p1f1
MRI-ESM2-0	r1i1p1f1
NESM3	r1i1p1f1
UKESM1-0-LL	r1i1p1f2

Bootstrap test

We use a bootstrap method to examine whether the difference of mean between sample A and sample B is statistically significant[43]. The sample A are re-sampled randomly to construct 10,000 realizations of mean standard deviation. In this random re-sampling process, any sample in sample A is allowed to be selected again. The same is carried out for the sample B. The 10,000 realizations of the sum of the two standard deviations can determine 95% confidence intervals for the difference of mean between sample A and sample B.

DATA AVAILABILITY

The ORAS5 data are available at https://cds.climate.copernicus.eu/cdsapp#!/dataset/reanalysis-oras5?tab=form. SODA2.2.4 data can be accessed at http://apdrc.soest.hawaii.edu/data/data.php. The CMIP6 data can be downloaded online https://esgf-node.llnl.gov/projects/cmip6/.

CODE AVAILABILITY

The codes that support the findings of this study are available from the corresponding author on request.

Received: 21 February 2023; Accepted: 7 August 2023;
Published online: 19 August 2023

REFERENCES

1. Alexander, M. A. et al. The atmospheric bridge: the influence of ENSO teleconnections on air-sea interaction over the global oceans. *J. Clim.* **15**, 2205–2231 (2002).
2. Timmermann, A. et al. El Niño–Southern Oscillation complexity. *Nature* **559**, 535–545 (2018).
3. Ren, H. L., Jin, F. F., Tian, B. & Scaife, A. A. Distinct persistence barriers in two types of ENSO. *Geophys. Res. Lett.* **43**, 10973–10979 (2016).
4. Liu, Z., Jin, Y. & Rong, X. A theory for the seasonal predictability barrier: threshold, timing, and intensity. *J. Clim.* **32**, 423–443 (2019).
5. Jin, Y., Liu, Z., He, C. & Zhao, Y. On the formation mechanism of the seasonal persistence barrier. *J. Clim.* **34**, 479–494 (2021).
6. Levine, A. F. Z. & McPhaden, M. J. The annual cycle in ENSO growth rate as a cause of the spring predictability barrier. *Geophys. Res. Lett.* **42**, 5034–5041 (2015).
7. McPhaden, M. J. Tropical Pacific Ocean heat content variations and ENSO persistence barriers. *Geophys. Res. Lett.* **30**, 1480 (2003).
8. Lopez, H. & Kirtman, B. P. WWBs, ENSO predictability, the spring barrier and extreme events. *J. Geophys. Res. Atmos.* **119**, 10114–10138 (2014).
9. van Oldenborgh, G. J., Balmaseda, M. A., Ferranti, L., Stockdale, T. N. & Anderson, D. L. Did the ECMWF seasonal forecast model outperform statistical ENSO forecast models over the last 15 years? *J. Clim.* **18**, 3240–3249 (2005).
10. Jin, E. K. et al. Current status of ENSO prediction skill in coupled ocean–atmosphere models. *Clim. Dyn.* **31**, 647–664 (2008).
11. Planton, Y. Y., Vialard, J., Guilyardi, E., Lengaigne, M. & McPhaden, M. J. The asymmetric influence of ocean heat content on ENSO predictability in the CNRM-CM5 coupled general circulation model. *J. Clim.* **34**, 5775–5793 (2021).
12. Larson, S. M. & Kirtman, B. P. Linking preconditioning to extreme ENSO events and reduced ensemble spread. *Clim. Dyn.* **52**, 7417–7433 (2019).
13. Dommenget, D., Bayr, T. & Frauen, C. Analysis of the non-linearity in the pattern and time evolution of El Niño southern oscillation. *Clim. Dyn.* **40**, 2825–2847 (2013).
14. Planton, Y., Vialard, J., Guilyardi, E., Lengaigne, M. & Izumo, T. Western Pacific oceanic heat content: a better predictor of La Niña than of El Niño. *Geophys. Res. Lett.* **45**, 9824–9833 (2018).
15. Larson, S. M. & Pegion, K. Do asymmetries in ENSO predictability arise from different recharged states? *Clim. Dyn.* **54**, 1507–1522 (2020).
16. Hu, J., Duan, W. & Zhou, Q. Season-dependent predictability and error growth dynamics for La Niña predictions. *Clim. Dyn.* **53**, 1063–1076 (2019).
17. Martinez-Villalobos, C., Newman, M., Vimont, D., Penland, C. & Neelin, D. Observed El Niño-La Niña asymmetry in a linear model. *Geophys. Res. Lett.* **46**, 9909–9919 (2019).
18. Geng, T., Cai, W., Wu, L. & Yang, Y. Atmospheric convection dominates genesis of ENSO asymmetry. *Geophys. Res. Lett.* **46**, 8387–8396 (2019).
19. Frauen, C. & Dommenget, D. El Niño and la Niña amplitude asymmetry caused by atmospheric feedbacks. *Geophys. Res. Lett.* **37**, L18801 (2010).
20. Chen, H. C. & Jin, F. F. Fundamental behavior of ENSO phase locking. *J. Clim.* **33**, 1953–1968 (2020).
21. Jin, Y. & Liu, Z. A theory of the spring persistence barrier on ENSO. Part I: The role of ENSO period. *J. Clim.* **34**, 2145–2155 (2021).
22. An, S. I. A review of interdecadal changes in the nonlinearity of the El Niño-Southern Oscillation. *Theor. Appl. Climatol.* **97**, 29–40 (2009).
23. An, S. I. & Jin, F. F. Nonlinearity and asymmetry of ENSO. *J. Clim.* **17**, 2399–2412 (2004).
24. Kang, I. S. & Kug, J. S. El Niño and La Niña sea surface temperature anomalies: Asymmetry characteristics associated with their wind stress anomalies. *J. Geophys. Res. Atmos.* **107**, 4372 (2002).
25. Suarez, M. J. & Schopf, P. S. A delayed action oscillator for ENSO. *J. Atmos. Sci.* **45**, 3283–3287 (1988).
26. Cai, W. et al. Changing El Niño–Southern Oscillation in a warming climate. *Nat. Rev. Earth. Environ.* **2**, 628–644 (2021).
27. Boucharel, J. et al. A surface layer variance heat budget for ENSO. *Geophys. Res. Lett.* **42**, 3529–3537 (2015).
28. Jin, F. F. & An, S. I. Thermocline and zonal advective feedbacks within the equatorial ocean recharge oscillator model for ENSO. *Geophys. Res. Lett.* **26**, 2989–2992 (1999).
29. Capotondi, A. et al. Understanding ENSO Diversity. *Bull. Am. Meteor. Soc.* **96**, 921–938 (2015).
30. Capotondi, A., Wittenberg, A., Kug, S. J. & Takahashi, K. ENSO diversity. *In El Niño Southern Oscillation in a changing climate*, **253**, 65–86 (John Wiley & Sons, Inc., 2020).
31. Xie, S. & Philander, S. G. H. A coupled ocean–atmosphere model of relevance to the ITCZ in the eastern Pacific. *Tellus* **46A**, 340–350 (1994).
32. Zhao, Y., Jin, Y., Li, J. & Capotondi, A. The role of extratropical Pacific in crossing ENSO spring predictability barrier. *Geophys. Res. Lett.* **49**, e2022GL099488 (2022).

33. Zuo, H., Balmaseda, M. A. & Mogensen, K. The new eddy-permitting ORAP5 ocean reanalysis: Description, evaluation and uncertainties in climate signals. *Clim. Dyn.* **49**, 791–811 (2017).
34. Carton, J. A. & Giese, B. S. A reanalysis of ocean climate using Simple Ocean Data Assimilation (SODA). *Mon. Wea. Rev.* **136**, 2999–3017 (2008).
35. An, S. I. & Kim, J. W. Role of nonlinear ocean dynamic response to wind on the asymmetrical transition of El Niño and La Niña. *Geophys. Res. Lett.* **44**, 393–400 (2017).
36. Jin, F. F. An equatorial ocean recharge paradigm for ENSO. Part I: Conceptual model. *J. Atmos. Sci.* **54**, 811–829 (1997).
37. Burgers, G. & Jin, F. F. & Van Oldenborgh, G. J. The simplest ENSO recharge oscillator. *Geophys. Res. Lett.* **32**, L13706 (2005).
38. Wang, P., Jin, Y. & Liu, Z. A diurnal predictability barrier for weather forecasts. *Mon. Wea. Rev.* **149**, 1715–1723 (2021).
39. Jin, Y., Liu, Z. & Duan, W. The different relationships between the ENSO spring persistence barrier and predictability barrier. *J. Clim.* **35**, 6207–6218 (2022).
40. Chen, M., Li, T., Shen, X. & Wu, B. Relative roles of dynamic and thermodynamic processes in causing evolution asymmetry between El Niño and La Niña. *J. Clim.* **29**, 2201–2220 (2016).
41. Hong, C. C., Li, T., LinHo & Kug, J. S. Asymmetry of the Indian Ocean dipole. Part I: Observational analysis. *J. Clim.* **21**, 4834–4848 (2008).
42. Eyring, V. et al. Overview of the coupled model intercomparison project Phase 6 (CMIP6) experimental design and organization. *Geosci. Model Dev.* **9**, 1937–1958 (2016).
43. Austin, P. C. & Tu, J. V. Bootstrap methods for developing predictive models. *Am. Stat.* **58**, 131–137 (2004).

ACKNOWLEDGEMENTS

This work is supported by Chinese NFSC 42206013 and the Fundamental Research Funds for the Central Universities.

AUTHOR CONTRIBUTIONS

Y.J. and H.C. designed the research. H.C. performed the analyses and wrote a draft of the paper. X.S., X.L. and R.H. discussed the results and made some suggestions. Y.J. and H.C. wrote the paper.

COMPETING INTERESTS

The authors declare no competing interests.

ADDITIONAL INFORMATION

Supplementary information The online version contains supplementary material available at https://doi.org/10.1038/s41612-023-00446-8.

Correspondence and requests for materials should be addressed to Yishuai Jin.

Reprints and permission information is available at http://www.nature.com/reprints

Publisher's note Springer Nature remains neutral with regard to jurisdictional claims in published maps and institutional affiliations.